Journal of Food Engineering 383 (2024) 112228

Contents lists available at ScienceDirect

Journal of Food Engineering

journal homepage: www.elsevier.com/locate/jfoodeng

Integration of oleaginous yeast-produced lipids into plant-based milk alternatives

K. Kramm [a,1,**], J. Heuer [b,1,*], V. Meunier [c], K. Haas [c], P. Arbter [b], S. Heinrich [a]

[a] Hamburg University of Technology, Institute of Solids Process Engineering and Particle Technology, Denickestraße 15, 21073, Hamburg, Germany
[b] Hamburg University of Technology, Institute of Bioprocess and Biosystems Engineering, Denickestraße 15, 21073, Hamburg, Germany
[c] Nestlé Research, Vers-Chez-Les-Blanc, Route du Jorat, 1005, Lausanne, Switzerland

ARTICLE INFO

Keywords:
Food powder
Emulsion
Spray drying
Homogenization
Fermentation
Oleaginous yeast
Single cell oil

ABSTRACT

In this study, the production of a novel oleaginous yeast-based milk powder alternative is presented. Three formulations, comprising yeast oil, oleaginous yeast cell lysate, and whole cells, were analyzed and compared to a reference formulation, covering the entire process from fermentation to powder analysis. The whole cell formulation exhibited highest encapsulating efficiency and low surface lipid content, indicating improved stability. Moreover, the formulation with cell lysate and whole cells showed larger oil droplet sizes in emulsions and spray-dried particles, and higher viscosity in rheological studies compared to the reference formulation. Electron microscopic images revealed morphological differences in spray-dried particles, emphasizing the impact of yeast oil integration. Concluding, formulations using oleaginous yeast present a complex system with diverse components. While this research pioneers oleaginous yeast integration into milk alternatives, further experiments are essential for a comprehensive understanding of observed effects and unlocking the full potential of these innovative and novel formulations.

1. Introduction

An increasing number of consumers are tending toward vegan milk alternatives (VMA) due to health, environmental, ethical, and animal welfare concerns (Cardello et al., 2022). Taking soy drinks as an example, cow's milk typically has around 2.2 times (Geburt et al., 2022) higher CO_2 emissions when the different energy content is taken into account and 3.5 times higher water requirements (Haas et al., 2019). However, regarding the nutritional value, alternatives like almond or oat drinks do not have preferable footprints compared to cow's milk (Geburt et al., 2022). Nevertheless, the plant-based product is gaining relevance in the food industry and an increasing industrial demand for VMA is projected to reach an estimated $24.6 billion by 2025 with an annual growth rate of 12.5% (Reyes-Jurado et al., 2023). To mimic and replace cow's milk, alternative protein, carbohydrate, and fat sources are needed. Depending on the choice of plant lipid in the formulation, the component can contribute to ecological issues.

In recent years, the importance of single cell oils has therefore increased (Di Fidio et al., 2021; Ochsenreither et al., 2016). They are produced in microorganisms such as yeasts or algae, which can achieve lipid contents of 20–70% based on cell dry weight during cultivation (Papanikolaou et al., 2011; Subramaniam et al., 2010). In addition to lipids, cellular components such as proteins, phospho- and sphingolipids, β-glucans, vitamins and antioxidants are also of interest for food formulations as they can contribute to functional properties, especially improved product stability, enhanced taste and nutritional value (Ali et al., 2019; Blomqvist et al., 2018; Caruso et al., 2022; Lourenço et al., 2019).

In comparison to other oleaginous microorganisms, oleaginous yeasts (OY) offer several advantageous features, including notably high specific growth rates and a wide range of substrate utilization capabilities (Athenaki et al., 2018). Furthermore, comprehensive knowledge regarding their cultivation, from well-established systems to industrial-scale applications, is readily available (Li et al., 2008; Meng et al., 2009).

The OY *Cutaneotrichosporon oleaginosus* is classified within the basidiomycetes division. Its nomenclature has undergone several revisions throughout the years. Historically, it was predominantly referred to as

* Corresponding author.
** Corresponding author.
E-mail addresses: Kathrin.kramm@tuhh.de (K. Kramm), jonas.heuer@tuhh.de (J. Heuer).
[1] K. Kramm and J. Heuer are equal contributors to this work and designated as co-first authors.

https://doi.org/10.1016/j.jfoodeng.2024.112228
Received 12 May 2024; Received in revised form 6 July 2024; Accepted 15 July 2024
Available online 26 July 2024

Candida curvata, *Apiotrichum curvatum*, *Cryptococcus curvatus* and *Trichosporon oleaginosus* (*Colombo* et al., *2011*; *Gujjari* et al., *2011*). Although today the valid taxonomic designation of this species is *Cutaneotrichosporon oleaginosus* (Di Fidio et al., 2021), outdated designations can still be found in strain libraries (see section 2.1.1).

Initially isolated from the drainage system of a dairy farm in 1978, the species was recognized for its potential as a promising producer of proteins and oils from diverse hydrolysates (Moon et al., 1978). Its foremost advantage lies in its rapid maximal growth rate (with a μ_{max} of up to 0.28 h^{-1}), its versatility in utilizing various carbon sources (Kourist et al., 2015), and its robust tolerance to inhibitory by-products associated with several hydrolysates (Yu et al., 2014a; Yu et al., 2014b). Notably, *C. oleaginosus* has demonstrated the capability to concurrently metabolize different C5- and C6-sugars along with various volatile fatty acids, such as acetate or propionate (Gong et al., 2016a,b; Yu et al., 2014a,b), as well as glycerol (Gong et al., 2016a,b).

Within the OY, approximately 90% of the synthesized lipids are stored within the cell in the form of triacylglycerols (TAGs) (Beopoulos et al., 2011). Smaller fractions of lipids in OY include less polar steryl-esters, lipophilic proteins, and phospholipids.

TAGs accumulate within specialized cellular compartments known as lipid bodies (Zweytick et al., 2000). The composition of TAGs in OYs exhibits variability among distinct strains and is profoundly influenced by the conditions of cultivation. Typically, the primary fatty acids include palmitic acid (C16:0), stearic acid (C18:0), oleic acid (C18:1), and linoleic acid (C18:2), with smaller proportions of myristic acid (C14:0), palmitoleic acid (C16:1), α-linolenic acid (C18:3), and longer-chain fatty acids (Beopoulos et al., 2011). This characteristic renders lipids obtained from OYs a promising alternative to many conventional plant-derived lipids, such as palm oil or cocoa butter (Sitepu et al., 2013; Wei et al., 2017). To proof this point, palm oil is taken as an additional reference for the yeast oil in the present work. It is worth noting that, even without genetic manipulation, the lipid composition can be influenced by various process parameters, including pH and dissolved oxygen levels. Additionally, the choice of yeast strain and substrate also exerts a crucial impact on the resulting lipid profile.

However, extraction and purification of oil from OY is challenging, less established and subsequently more costly today as compared to plant derived oils. Using the whole OY biomass in food formulation, is a pathway to reduce the application cost and might lead to additional benefits due to other non-lipid OY fractions such as proteins and cell-wall hydrocolloids which can deliver nutrients and desired functional properties.

In this first-of-its-kind report, we explored the use of OY biomass as a lipid source for VMA emulsion and powders for the very first time and characterized the resulting VMA properties.

VMA are usually oil-in-water (O/W) emulsions in which the dispersed oil phase is present as droplets in the continuous water phase. Plant proteins which are used instead of dairy proteins are used to form and stabilize the emulsion (Armbruster et al., 1991; Leal-Calderon et al., 2007). The proteins accumulate at the phase interface between the oil and water phases, reducing the interfacial tension. In the food industry, mechanical homogenization techniques are often used to optimize product properties such as reduced droplet size distribution (Kivelä et al., 2010). Dried VMA in powder form is produced to substitute partially or complete dairy powders which are currently used in various areas. They usually provide better physical and chemical stability, easy handling, efficient transport and low storage volume compared to the liquid food product. Spray-drying is the most common technique to produce VMA powders due to its limited heat impact (Romulo, 2022). However, during spray-drying, the lipids are usually only partially integrated and protected by the powder matrix. Consequently, a significant fraction of the non-encapsulated oil is present on the article surface which can lead to powder oxidation and other stability challenges. Moreover, spray-drying is limited to medium viscosity liquids and can be challenging for materials with significant fraction of insoluble material.

In this study, a VMA was produced with different integration forms of OY. The aim was not only to use the oil produced by the yeasts but also to implement the beneficial by-products such as vitamins, proteins, antioxidants and fiber into the VMA product. The yeast product forms like purified yeast oil, cell lysate and whole cells, which have not yet been incorporated into VMA products, were compared with the reference sunflower oil formulation used and analyzed by Kramm et al. (2024). Based on the investigation of the lipid properties, the characteristics of the VMA emulsion and powder are to be identified and correlations demonstrated.

2. Material and methods

2.1. Materials

2.1.1. Strain and media

The strain listed as *Trichosporon oleaginosus* DSM 11815 (DSMZ, Germany) was cryogenically preserved at −80 °C in a growth medium containing lysogeny broth Lennox (LB) by Carl Roth (Germany) and 25% glycerol as a cryoprotectant. For the preparation of pre-cultures, a 2 mL aliquot from the cryogenically stored culture was used to inoculate 50 mL of LB medium. After 24 h in the first pre-culture, 25 mL was employed to inoculate a second seed culture, resulting in a final volume of 250 mL. This second seed culture was established using LB medium supplemented with an additional 30 g/L of glucose. After an additional 24 h, the second culture was employed to inoculate the main bioreactor cultures. In this step, 1 L (equivalent to 5% (v/v)) was used to reach a final volume of 20 L post-inoculation. The specific composition of the medium for the main culture is detailed in Tables 1 and 2. However, the initial batch medium was supplemented with various salts and trace elements, which are listed in Tables 1 and 2 The trace elements, phosphate salts and the glucose solution (500 g/L) were autoclaved separately and introduced after sterilization of the bioreactor. The initial glucose concentration in the fermentation was 70 g/L. Before reaching a high cell population ($OD_{600} > 100$) with a low risk of contamination, sterile glucose solution was used as a feed. Afterwards, solid glucose monohydrate was fed.

2.1.2. Cultivation system and conditions

Cultivation was conducted in a 30 L bioreactor from Bioengineering (Switzerland), with a working volume of 20 L. The bioreactor was equipped with pH and pO2 probes manufactured by Mettler-Toledo (Switzerland). The pH was controlled at 6.5 through automated addition of 5 M NaOH. The temperature was maintained at a constant 30 °C. Prior to cultivation, the probes and fermenter pumps underwent calibration, and the bioreactor was sterilized at 121 °C for 20 min under 1 bar of overpressure. Initial conditions involved running the bioreactor at 400 revolutions per minute (rpm) and providing aeration with air at a rate of 1 vvm (volume of air per volume of liquid per minute). Over the course of fermentation, the rpm was progressively increased to a maximum of 1200 rpm, and aeration was raised to 3 vvm to enhance the oxygen transfer rate (OTR).

Table 1
Media composition of the defined medium for *C. oleaginosus* cultivation.

Component	Concentration [g/L]
KH_2PO_4	1.06
Na_2HPO_4	1.00
$MgSO_4 \cdot 7H_2O$	1.50
$(NH_4)_2SO_4$	6.00
Trace element solution	10 mL

Table 2
Composition of the trace elements solution.

Component	Concentration [g/L]
$ZnSO_4 \cdot 7H_2O$	0.10
$FeSO_4 \cdot 7H_2O$	0.55
$CaCl_2 \cdot 2H_2O$	4.00
$MnSO_4 \cdot H_2O$	0.076
$ZnSO_4 \cdot 7H_2O$	0.10
H_2SO_4 (5 M)	0.10 mL

2.1.3. Cell growth

Cell growth was monitored through the measurement of optical density at 600 nm (OD_{600}). To achieve an optical density falling within the range of 0.1–0.4 units at 600 nm, samples from the bioreactor were appropriately diluted. The determination of biomass dry weight (BDM) was carried out using a gravimetric method involving cell pellets obtained from 2 mL of the culture broth, which were then dried at 70 °C for 24 h. These pellets were obtained through a 5-min centrifugation at 16,242×*g*. In cases where cells did not form a solid pellet after centrifugation due to their high lipid content, the cell dry weight was determined using only 1 mL of the culture broth. In these instances, 1 mL of 70% ethanol was added to the sample, which was then subjected to centrifugation. This process facilitated the formation of a solid pellet, even when dealing with high-lipid-content cells.

2.1.4. Quantification of glucose

To quantify glucose, we employed an HPLC system (Kontron, UK). Separation was carried out using the Aminex HPX-87H column at temperatures of either 60 °C, with a flow rate of 0.6 mL/min and a mobile phase consisting of 0.2% (v/v) trifluoroacetic acid. Glucose was detected using a refractive index (RI) detector. The process involved centrifuging cells at 16,242×*g* for 5 min, followed by filtration of the supernatant through a 0.2 μm PVDF filter. Sample dilutions were performed to ensure concentrations falling within the range of 50-5000 mg/L for individual sugars, in accordance with the established method's linear range.

2.1.5. Lipid analytics

For the quantification of lipids, a 50 mL sample of the culture broth was subjected to centrifugation at 7000×*g* for 10 min at 4 °C, and the resulting supernatant was discarded. The cell pellet was then freeze-dried for a duration of 72 h. Subsequently, fatty acid methyl esters (FAMEs) were generated through a direct transesterification protocol (as outlined by (Arbter et al., 2019; Griffiths et al., 2010). Subsequently, for FAME quantification, gas chromatography equipped with a flame ionization detector (GC-FID) was used. Each sample was extracted in triplicate, and, if necessary, samples were diluted with hexane to fit within the linear range of the developed method. Gas chromatography was performed using a GC2030 gas chromatograph (Shimadzu, Japan) equipped with a SH-PolarD column (30 m × 0.32 mm x 0.50 μm). The injection volume was 1 μL, and the injector temperature was set at 220 °C. Injection was conducted in split mode with a split ratio of 20. The carrier gas employed was nitrogen, with a constant linear velocity of 25 cm/s. The initial column temperature was 100 °C and held for 4 min. Subsequently, the column temperature was increased at a rate of 25 °C per minute to 200 °C and held for an additional 8 min. Finally, the temperature was further increased at a rate of 5 °C per minute to 250 °C, which was maintained for 12.5 min. The FID was configured to 260 °C with a sampling rate of 40 ms, utilizing nitrogen as the makeup gas at a flow rate of 24 mL/min. Calibration was conducted using the AOCS FAME-Standard No. 6 (RM-6). Finally, the concentration of the respective FAMEs in the samples was obtained with help of the calibration and divided by the amount of used biomass. From this, the lipid content of the cells was obtained.

2.1.6. Beta-glucan

In accordance with the commercial kit for the enzymatic quantification of yeast β-glucan (K-EBHLG, Megazyme) this assay was conducted. Approximately 20 mg of accurately weighed samples were suspended in 0.4 mL of 2 M KOH and stirred in an ice–water bath for 30 min. Subsequently, 1.6 mL of 1.2 M sodium acetate buffer at pH 3.8 was added with mixing, followed by the addition of 40 μL of an enzyme mixture, comprising exo-1,3-β-glucanase, endo-1,3-β-glucanase, β-glucosidase, and chitinase. The mixture underwent incubation at 40 °C for 16 h. Following this, 10 mL of water was introduced to the tube with mixing, and the tubes were centrifuged at 1821×*g* for 10 min. Aliquots of 0.1 mL were extracted for glucose determination using an enzyme mixture, comprising glucose oxidase plus peroxidase. Concurrently, glucose standards and reagent blanks were run at 510 nm for comparison. To avoid counting intra- and extracellular glucose as β-glucan, the glucose measured in cell lysate according to 2.1.4 was subtracted.

2.1.7. Whole cells and cell lysate preparation

Upon completion of the fermentation process, the fermentation broth was carefully collected and preserved by storing it in a freezer at −20 °C. To obtain a powder form of whole cells, the broth was subjected to freeze-drying at −42 °C and 0.010 bar for a duration of 72 h. To produce cell lysate powder, the broth underwent a homogenization process involving five cycles at 2000 bars, utilizing a PandaPLUS Lab Homogenizer 2000 (GEA, Germany), followed by freeze-drying at −42 °C and 0.010 bar for 72 h.

2.1.8. Yeast oil extraction

The oil was extracted from the acquired cell lysate powder using a supercritical CO_2 extractor, the SFE Lab 100 mL system from SFE Process (France). The extraction was conducted at 200 bar and 50 °C, employing a CO_2 flow rate of 60 g/min. Subsequently, the extracted oil was preserved at a temperature of −20 °C.

2.1.9. Differential scanning calorimetry

The thermal characteristics of palm, sunflower and yeast oil, contained within hermetically sealed aluminum pans, were analyzed using an DSC 25 (TA Instruments, USA). The samples underwent a cooling process to −60 °C at a rate of 5 °C/min and were kept at that temperature for 10 min isothermally. Subsequently, they were heated to 50 °C at a rate of 5 °C/min. The cooling and heating procedure was repeated and the second heating thermograms were analyzed. The obtained thermograms were used to determine the total melting enthalpy (ΔH) and absolute melting energy (E). ΔH is expressed as energy per sample mass (in J/g), while *E* represents the energy (in J) consumed by the sample mass. The solid fraction of the samples was estimated via a formula involving the partial integration of thermograms at various temperatures (Márquez et al., 2013):

$$solid\ fraction = \frac{\int_{T}^{T_f} Edt}{\int_{T_0}^{T_f} Edt} \quad (1)$$

2.1.10. Integration in vegan milk alternatives

To further investigate the influence of the altered lipid source and its state form, a model system was used. The model represents a possible system for a VMA emulsion as well as powder and consists besides the used lipid of glucose syrup with a dextrose equivalent (DE) of 21, soy protein isolate and oat bran. The reference formulation is Y0 (see Table 3), where sunflower oil is used as the lipid. In the remaining formulations, the yeast oil is either extracted (Y1), present in the cell lysate (Y2), or encapsulated in the yeast cells (Y3).

The raw material Glucidex DE 21 (Azelis, Germany) was used for the amorphous polysaccharide glucose syrup DE 21. Soy protein isolate from the VEGACON® 90S product line (Eurosoy, Germany) served as the protein source and was characterized by a crude protein content in

Table 3
Overview of the formulations Y0, Y1, Y2 and Y3 used in the study with their raw material compositions.

Formulation	Y0	Y1	Y2	Y3
Glucose syrup DE 21 [%]	66	66	51	52
Soy protein isolate [%]	20	20	16	16
Oat bran [%]	4	4	3	2
Sunflower oil [%]	10	/	/	/
Yeast oil [%]	/	10	/	/
Cell lysate [%]	/	/	30	/
Whole cells [%]	/	/	/	30

dry matter of 91.3% and an ash content of 4.55% with moisture content of the raw material of 5.8 g/100g. The fiber β-glucan was introduced into the model system through the raw material oat bran (Mühle Schlingemann, Germany). The oat bran had a β-glucan content of 4.5 g/100 g, fiber fraction of 11.4 g/100 g, protein content of 138 g/kg and a Total Kjedahl Nitrogen of 22 g/kg. To maintain a constant oil concentration and an equal proportion of fiber and protein in all formulations, the prepared cell lysates and whole cells were adjusted based on their composition (see Table 4). Emulsion preparation was performed in duplicates with a total solid content of 30% to demineralized water for all formulations (see Table 5).

2.1.11. High-pressure homogenization

Depending on the formulations, a crude emulsion was prepared by adding the raw materials to the water phase and pre-homogenizing with the T 50 Ultra Turrax high-performance disperser (IKA, Germany) at an intensity of 6000 rpm for 10 min. Subsequently, high-pressure homogenization was performed with the TwinPanda 600 (GEA, Germany). The two-stage laboratory homogenizer was operated at a pressure of 450/150 bar with one passage and an inlet temperature of 20 °C. The heat generated by the process increased the temperature of the emulsion after the passage to 34–41 °C. The temperature range is a result of the different characteristics of the VMA formulations.

2.1.12. Spray-drying

After high-pressure homogenization, the VMA emulsions were dried in the laboratory spray dryer B-290 (Büchi Labortechnik AG, Switzerland). The spray dryer operated in co-current principle. The emulsion is atomized by a two-fluid nozzle with an external liquid mixture, the liquid insert had a diameter of 0.7 mm to the total cap diameter of 1.5 mm. For each formulation, 600 mL of emulsion volumes were processed at a constant spray rate of 10 g/min, an input temperature of 220 °C, and an output temperature between 120 and 85 °C. The aspirator was operated at 85%, which corresponds to a volume flow of 33 m^3/h. On the rotameter, a spray gas flow rate of 40 mm was set, correlating to a flow rate of 667 L/h. The powder production was conducted in duplicates for each formulation.

2.2. Analysis of emulsion properties

2.2.1. Droplet size distribution

To determine the droplet size distribution before and after homogenization, the Mastersizer 3000 (Malvern Panalytical, United Kingdom) was used. Sedimentation or separation of sample in the water dispersant was prevented in the wet dispersion unit by operating a stirrer at a rotational speed of 1600 rpm. To avoid measurement deviations, the sample concentration was kept constant within an obscuration range of 0.5–8.0% and measured in at least triplicates. The evaluation of the droplet size distribution was based on the Mie theory (Mie, 1908) assuming spherical oil droplets. The light microscope BX51 (Olympus, Germany) was used for the detection of droplet aggregation and microscopic images were captured at a magnification of 50x.

Table 4
Overview of the cell lysate and whole cell compositions.

Component [%]	Cell lysate	Whole cells
water	7.22	10.39
protein	5.73	5.76
glucose	24.14	22.39
β-glucan	3.38	5.23
fat	29.65	29.65

Table 5
Characteristic droplet size parameters of the different VMA emulsion formulations depending on high-pressure homogenization.

Formulation/ Pressure [bar]		$x_{10,3}$ [μm]	$x_{50,3}$ [μm]	$x_{90,3}$ [μm]	$x_{3,2}$ [μm]	$x_{4,3}$ [μm]	SPAN [−]
Y0	Pre	4.7 ± 0.7	29.1 ± 5.2	73.0 ± 10.4	12.2 ± 3.2	34.7 ± 4.5	2.3 ± 0.2
	450/150	0.3 ± 0.0	5.7 ± 0.5	62.4 ± 8.6	1.0 ± 1.4	18.5 ± 1.8	2.9 ± 0.1
Y1	Pre	8.2 ± 4.1	41.2 ± 10.2	138.0 ± 29.4	17.2 ± 8.5	58.8 ± 12.4	3.2 ± 2.1
	450/150	0.3 ± 0.0	9.8 ± 4.2	114.0 ± 20.1	1.2 ± 0.4	33.1 ± 7.9	11.6 ± 3.5
Y2	Pre	10.2 ± 1.0	69.5 ± 7.3	219.0 ± 26.8	23.8 ± 5.8	158.0 ± 15.3	3.0 ± 1.1
	450/150	5.1 ± 0.1	11.1 ± 0.3	19.2 ± 4.6	8.8 ± 2.5	11.7 ± 3.7	1.3 ± 0.2
Y3	Pre	3.6 ± 0.2	60.6 ± 6.1	143.0 ± 7.4	12.3 ± 4.1	66.2 ± 6.9	2.3 ± 1.0
	450/150	3.2 ± 0.0	7.6 ± 0.1	18.9 ± 0.8	6.1 ± 0.3	9.5 ± 0.7	2.0 ± 0.1

2.2.2. Light microscopy

For light microscopy image acquisition of the emulsions before and after the homogenization, a Nikon eclipse 80i with a camera (Digital sight D) was used. With a magnification of 100-fold, the images were randomly selected.

2.2.3. Zeta potential

For the identification of possible differences in emulsion stability, the zeta potential was determined with the Zetasizer Nano ZS (Malvern Panalytical, United Kingdom). To avoid multiple scattering due to excessive sample concentration and the resulting inaccuracies of the measurement results, the sample was diluted 1:50 with demineralized water. The zeta potential was measured in triplicates using DTS1070 cuvettes (Malvern Panalytical, United Kingdom) and evaluated as a function of pH value, which was recorded using inoLab pH 7110 m (WTW, Germany). To ascertain the isoelectric point, the pH value was adjusted with 0.1 M HCl solution.

2.2.4. Rheological investigation

The dynamic viscosity of the emulsion was measured using a Kinexus Pro rheometer (Malvern Panalytical, United Kingdom) applying rotational measurements using a cone and plate geometry at 25 °C. The cone geometry had a cone angle of $\alpha = 1.012°$ and a diameter of 60 mm. The sample volume used was 1.01 mL with a gap distance between geometries of 0.031 mm. During the measurement, the sample was stressed in a shear rate range between 1 and 1000 s^{-1} with 6 data points per decade. Viscosity curves were created in the upward and downward direction for the double-produced emulsions per formulation.

2.2.5. Interfacial tension measurement

The K100 Force Tensiometer (Krüss, Germany) was used to determine the interfacial tension and identify the lipid influence on the stabilization. The measurement was performed in duplicates with the du Noüy ring method at a temperature of 20 °C. The immersion depth of the ring during the measurement was 8 mm, with a measuring speed of 2 mm/min and a sensitivity of 0.0001 g. The interfacial tension γ depends on the maximum force at the elongation of the liquid lamella F, the

wetted length L and the phase angle θ:

$$\gamma = \frac{F}{L \bullet \cos\theta} \tag{2}$$

2.3. Analysis of particle properties

2.3.1. Particle size measurements

For the identification of particle shape and size distribution, the CamSizer XT (Retsch Technology, Germany) was used, which employs the dynamic image analysis method based on the 2-camera principle. Due to the powder composition, the measurement was performed with compressed air dispersion and a dispersion pressure of 90 kPa. The parameter sphericity S was calculated according to ISO 9276-6:

$$S = \frac{4 \bullet \pi \bullet A}{P^2} \tag{3}$$

The measured area covered by the particle protection is represented by A, whereas P indicates the measured perimeter of a projection. The Sauter mean diameter was determined based on the particle size distribution using the software Matlab and corresponds to the particle diameter of a monodisperse material system, with a total volume and surface area equal to the polydisperse system. Each measurement was repeated at least three times to ensure repeatability.

2.3.2. Moisture content

To ascertain the moisture content of the VMA powder after the spray drying process, the EM 120-HR moisture analyzer (Precisa Gravimetrics AG, Switzerland) was used. The measurement is based on thermogravimetry at a temperature of 102 °C for 30 min. To ensure repeatability, the measurement was repeated at least three times for all produced powders.

2.3.3. Particle density and closed porosity

The particle density was determined using the AccuPyc 1330 helium pycnometer (Micromeritics, United States). The fraction of closed pores in the powder was also determined using the AccuPyc 1330 helium pycnometer (Micromeritics, United States). For each powder produced, six individual measurements were performed. The closed porosity ε_{closed} was calculated from the apparent material density without processing ρ_s and after crushing the particles ρ_c with a mortar to destroy the internal voids:

$$\varepsilon_{closed} = 1 - \frac{\rho_s}{\rho_c} \tag{6}$$

2.3.4. Surface lipid analysis

The analysis of surface lipids was conducted to evaluate the encapsulation effectivity and for the estimation of potentially occurring oxidation processes. 2 g of VMA powder was dispersed in 40 mL of n-heptane. To ensure optimal lipid extraction from the particle surface, the dispersion was stirred at 300 rpm for 10 min by a laboratory vibrator. After a sedimentation phase lasting 30 min, the liquid supernatant was separated from the solid particles. The supernatant was subjected to a subsequent centrifugation step at 809×g for 5 min to remove remaining powder particles. The liquid phase was collected with a syringe and cleaned from particulate components by a sterile filter. The filtrate was filled with a volume of 25 mL onto pre-weighed aluminum pans and the solvent in the pans was evaporated on a heating plate at 115 °C. Once evaporation was complete, the pans were heated for an additional 10 min. Followed by a drying process at 100 °C for 30 min in a heating oven and cooling in a desiccator with silica gel for at least 1 h. The concentration of the surface lipids and the encapsulation effectivity were determined by weighing the aluminum pans regarding the powder moisture content. The encapsulation efficiency (EE) is defined by the mass differences of the total lipid content m_{TL} from the fraction located on the surface m_{SL} in relation to the total oil content:

$$EE = \frac{m_{TL} - m_{SL}}{m_{TL}} \tag{7}$$

The analysis was performed in triplicates.

2.3.5. Electron microscopy

The scanning electron microscope Zeiss Supra VP 55 (Carl Zeiss, Germany) was used for the morphological characterization of the VMA formulations. To prevent charge accumulation during the examination, the samples are attached to a self-adhesive carbon carrier and coated with gold. The thickness of the gold layer was between 7 and 8 nm. The analysis was conducted under a vacuum pressure of $1.6*10^{-6}$ mbar in the sample chamber, with an electron acceleration voltage of 2 kV. Images of the VMA powder samples were captured at a magnification of 3kx, using an aperture size of 30 μm and a working distance of 10–11 mm.

3. Results and discussion

3.1. Cultivation of Cutaneotrichosporon oleaginosus

To avoid the inhibitory effects of a high glucose concentration, a fed-batch culture method was conducted. In Fig. 1 the times of the feeding are shown. After 12 h (1.), the equivalent of 1500 g glucose was fed as sterile solution. After 30.75 h (2.) and 34.75 h (3.) the equivalent of 1000 g glucose was fed as solid glucose monohydrate, respectively. In total, 4900 g glucose was fed into the bioreactor. Subtracting the remaining glucose after 97 h, 4620 g glucose was consumed. This leads to an overall biomass yield of 0.42 g BDM per g glucose, an overall lipid yield of 0.12 g per g glucose and an overall lipid production rate of 0.28 g/(L*h). The lipid yield per gram of glucose is low compared to the 19.1–21.8 g of lipids per gram of glucose observed in shaking flask experiments, depending on the C/N ratio (Koivuranta et al., 2018). This could be due to the feeding strategy (batch vs. fed-batch) and a higher glucose concentration.

The typical trend of glucose and biomass concentrations and lipid content are presented in Fig. 1. Initially, the cell growth was very rapid, the biomass increased to 55.67 g/L within the first 22.75 h. Before this sample, the lipid content was below 0.1 g/g biomass, indicating that glucose was not used for lipid storage molecules but membrane biosynthesis. From the 23rd to the 70th hour, lipid accumulated quickly. At this time the ammonia concentration went down to zero, triggering

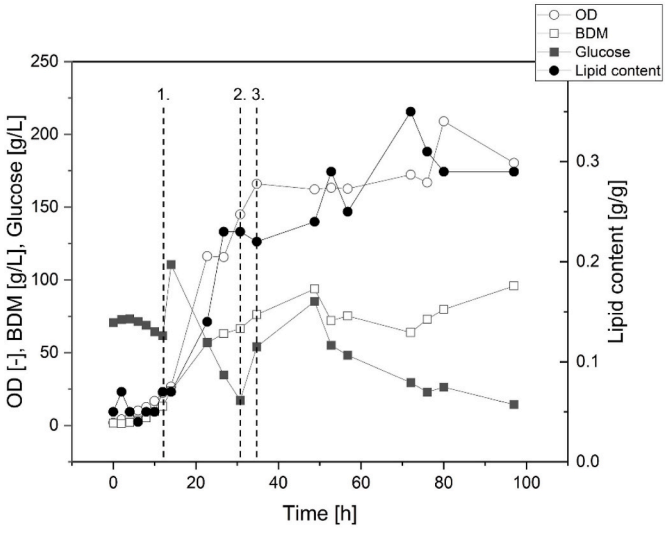

Fig. 1. Fed-batch fermentation profile of *C. oleaginosus* in a 30 L bioreactor showing the OD_{600}, BDM and glucose concentration and the lipid content of the yeast cells.

the storage of excessively available glucose in form of TAGs under nitrogen limitation (Aliyu et al., 2021). A lipid content peak of 0.35 g/g was reached and afterwards, in the final phase of the fermentation, the results indicate that a lipid content reduction took place, possibly because of the yeast's utilization as a reserve storage of carbon and energy due to a lower concentration of available glucose.

3.2. Preparation of yeast materials

After 97 h, the fermentation broth was harvested and divided into three parts for the preparation of dried whole cells, dried lysed cells and yeast oil. The untreated whole cells were freeze dried directly, the lysed cell powder was prepared by disrupting the cells mechanically via homogenization followed by freeze-drying. The yeast oil was extracted from the lysed cell powder using supercritical carbon dioxide extraction. Photos of the three obtained products are displayed in Fig. 2.

3.3. Lipid analytics

The oil extracted from the harvested yeast, as well as the sunflower oil and the palm oil, underwent composition analysis via GC-FID, and the findings are presented in Fig. 3. All oils primarily comprise long-chain fatty acids containing 16 and 18 carbon atoms. Predominantly, the palm and yeast oil have a higher fraction of saturated fatty acids, palmitic and steric acid, compared to the sunflower oil. On the other side, sunflower oil consists out of 58% linoleic acid while around 10% were measured in palm and yeast oil. The values indicate that the yeast oil could rather act like a palm oil equivalent than a sunflower oil equivalent but still offers a higher fraction of unsaturated fatty acids, mainly oleic acid.

Fig. 4 shows the melting behavior of the three different oils analyzed. As expected, due to the high amount of polyunsaturated fatty acids (58% linoleic acid), the sunflower oil melts at low temperature within a range of −29 °C and −17 °C in a steep melting curve. Interestingly, and possibly rooted in a similar ratio between saturated and mono-unsaturated fatty acids, the palm oil and the yeast oil show a comparable melting performance. While the palm oil starts to melt at 0 °C until 37 °C, whereas the solid fraction goes down from 0.9 to 0.1 in between 13.5 °C and 22.9 °C, the yeast oil shows a steeper melting curve starting at 10 °C and ending at 21 °C (see Fig. 8, Fig. 9).

3.4. Influence of yeast oil on the emulsion characteristics

3.4.1. Droplet breakup

Since the emulsion properties have a major influence on the final particle characteristics after the spray drying process, the droplet size distribution was analyzed before and after homogenization with the high-pressure homogenizer. Fig. 5 shows the volume density distributions of the various VMA emulsion formulations depending on the homogenization pressure. The VMA formulations with incorporated sunflower oil (Y0) and yeast oil (Y1) result in significantly smaller

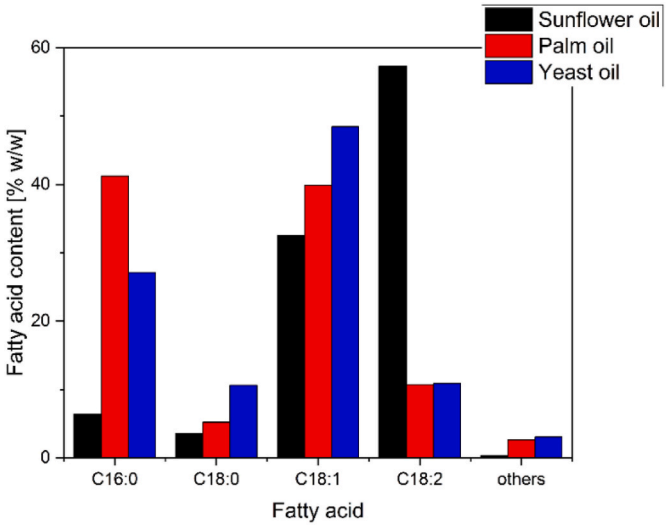

Fig. 3. Fatty acid profiles of sunflower oil, palm oil and yeast oil from *C. oleaginosus*.

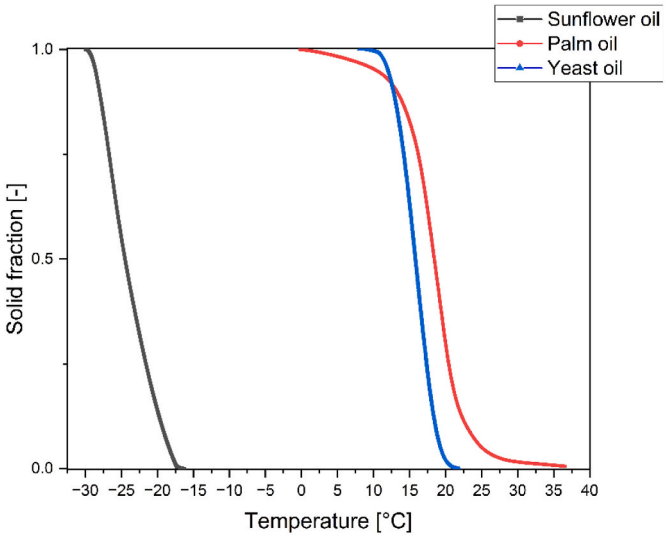

Fig. 4. Melting curves of sunflower, palm and yeast oil estimated from DSC thermograms.

droplet diameters after processing. Considering 3.1.3, an influencing parameter is the lower dynamic viscosity values of the formulations compared to the integration form with the cell compartments. The compositions Y0 and Y1 also have a broader droplet size distribution. In the analysis by Hu et al. (2003), the application of soy protein isolate as

Fig. 2. Yeast materials produced from *C. oleaginosus* to be formulated in alternative milk powders. From left to right: whole cells, lysed cells and oil.

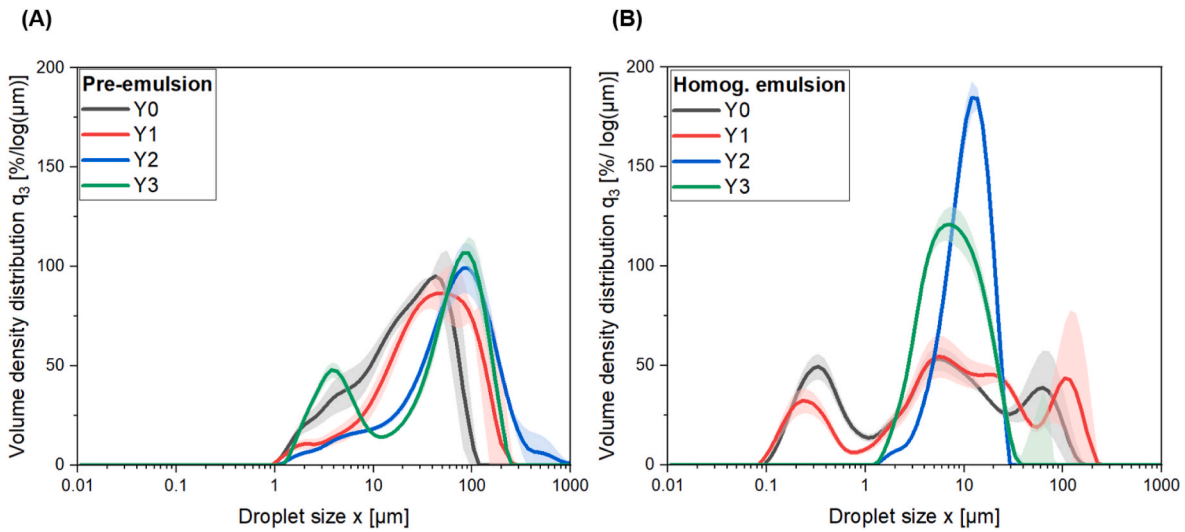

Fig. 5. Volume density distribution of the different VMA emulsion formulations (A) before and (B) after processing in the high-pressure homogenizer.

an emulsifier system for the production of an O/W emulsion after homogenization led to a bimodal distribution at concentrations of 0.2 and 0.5% protein. Based on the component analysis (see Fig. 10), the distribution width can be attributed according to the investigations of Kramm et al. (2024) to the comminution of the oil droplets and the fragmentation of the oat bran. The incorporation of yeast oil into the formulation (Y1) results in larger droplet diameters compared to the reference with sunflower oil (Y0), whereby the altered lipid properties of yeast oil result in more impeded droplet break-up. These correlations are confirmed by the light microscope images of the formulations in Figs. 6 and 7 before and after processing with the high-pressure homogenizer. The distribution of oat bran and soy protein isolate in the emulsion formulations can be found for a similar system of vegan milk alternatives in Kramm et al. (2024). A maximum occupancy of the emulsifier at the interface can be assumed based on the used emulsifier concentration (comparison Table 3), as a low saturation concentration of soy protein isolate at the droplet surface was found in the studies by Hu et al. (2003). The homogenization of Y2 reduces the droplet diameter and the distribution width. The fragments of the cell lysate already formed during cell disruption were further comminuted by the processing step during emulsion formation, as can be seen in Fig. 10. Thus, the lysate form of the yeast cells affects the homogenization result in addition to the reduction of the oat bran, protein aggregates and oil droplets. In formulation Y3, the proportion of coarse material is primarily reduced by homogenization and thus also the distribution width. Fig. 10 shows that the whole cells are not damaged by the applied homogenization pressure, therefore the minimum droplet diameter remains approximately constant. The oat bran and any aggregates are thus crushed in the formulation, which is confirmed by the light microscope images. The integration of yeast oil in the formulation shows instabilities and aggregate formation which can be attributed to the different lipid properties compared to sunflower oil (see section 3.3)

3.4.2. *Zeta potential analysis*

In the VMA formulations, the proteins act as emulsifiers and stabilize the disperse phase in the O/W emulsion by introducing an electrical charge (Hu et al., 2003) (see Table 6). The electrostatic repulsive forces outweigh the steric interactions if proteins are used, as the adsorption of the emulsifying component only leads to low layer thicknesses at the interface (Zhang et al., 2021). To estimate the effect of the integration form of the yeast oil (Y1–Y3) on the emulsion stability compared to the reference with sunflower oil (Y0) after high-pressure homogenization, the zeta potential was determined. Fig. 11 shows the relation between the zeta potential and the pH value. The zeta potential decreases from the acidic to the basic pH range for all formulations. This correlation is also described in the studies of Tomczynska-Mleko et al. (2014). The incorporation of yeast oil into the VMA formulation results in different potential values. This correlation suggests that the yeast oil has a destabilizing effect due to the different composition compared to the reference emulsion with sunflower oil and thus confirms the findings in 3.4.1. In investigations by O'Flynn et al. (2021), the zeta potential of soy protein isolate dispersions was determined as a function of the pH value. The generated data by O'Flynn et al. (2021) is similar to the measured values of Y0 in this work. Due to the multi-component formulation, deviations from the isoelectric point of the soy protein isolate, pI 4.6, (O'Flynn et al., 2021; Wolf, 1970) are recognizable. The influence of the

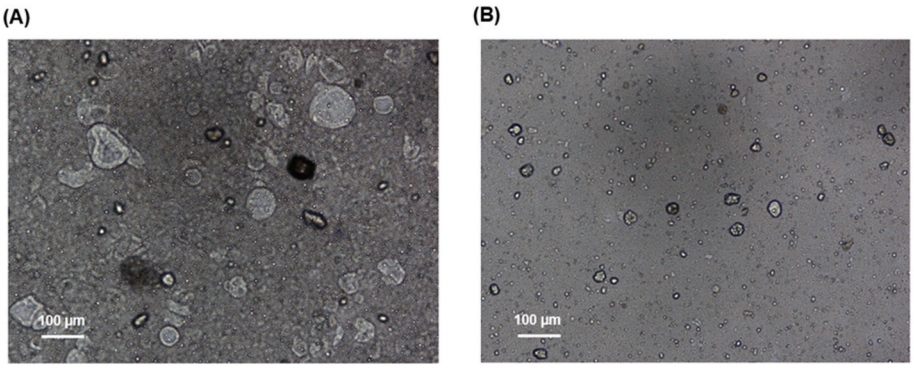

Fig. 6. Light microscope image of the VMA formulation Y0 with sunflower oil (A) before and (B) after processing in the high-pressure homogenizer.

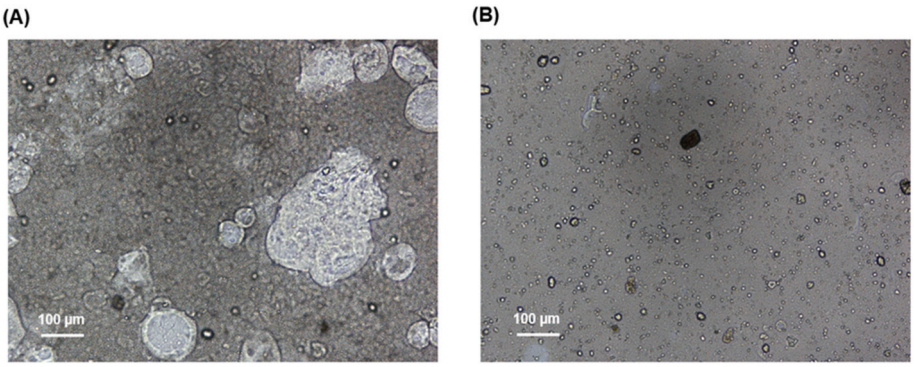

Fig. 7. Light microscope image of the VMA formulation Y1 with yeast oil (A) before and (B) after processing in the high-pressure homogenizer.

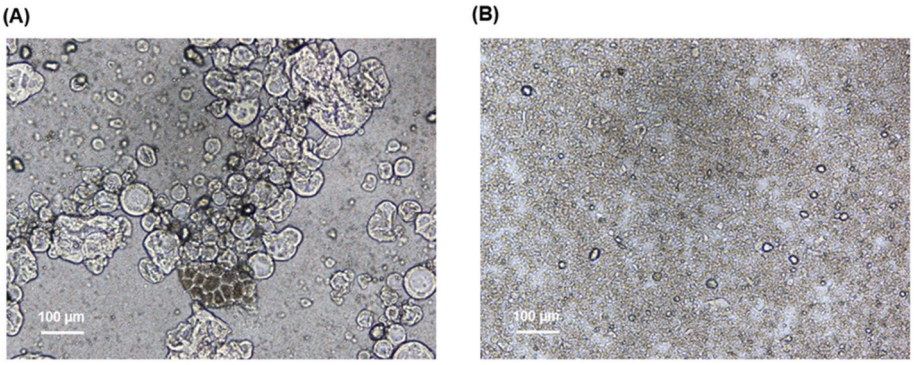

Fig. 8. Light microscope image of the VMA formulation Y2 with cell lysate (A) before and (B) after processing in the high-pressure homogenizer.

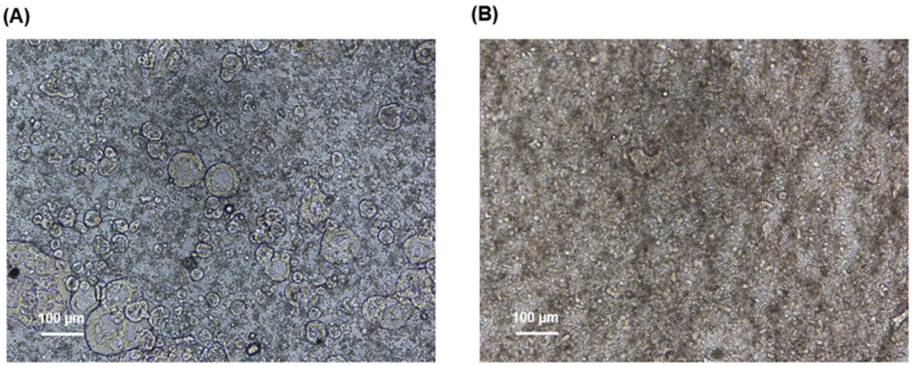

Fig. 9. Light microscope image of the VMA formulation Y3 with whole cells (A) before and (B) after processing in the high-pressure homogenizer.

remaining formulation components is therefore higher for compositions Y1, Y2 and Y3 compared to reference Y0. The samples of the zeta potential measurement could not be adjusted in a constant pH range due to the lower solubility and precipitation of the proteins in an acidic environment. Especially under extremely acidic conditions, the tertiary and quaternary structure of the subunits of soy protein isolate β-conglycinin and glycinin are altered and influence the emulsion properties, for example through alternative protein-protein interactions (O'Flynn et al., 2021). Differences can also be seen between Y2 and Y3, whereby the whole cells exhibited a more negative zeta potential at each tested pH. Consequently, a more stable emulsion system can be expected compared to the formulation with cell lysate. As a result of cell disruption, the yeast proteins are present in the medium, so the influence of the pH value is greater than on the yeast proteins immobilized in the OY cells. In addition, the yeast cell wall has a potential and results in a negative surface charge (Kregiel et al., 2012; Stirke et al., 2019). The production of the cell lysate destroys the cell wall and thus changes the surface charge. Especially in the acidic pH range, the integration form of the whole cells seems to result in the most stable system. Considering Table 7, the introduction of yeast oil and cell components reduces the pH value towards the acidic range. As in plant oils, free fatty acids cause an acidic pH in the yeast oil. For the whole cells and lysate, this aspect can be partly attributed to the cultivation conditions, as the yeast cells grew at pH 6.5.

For the spray drying process, the VMA emulsions without pH value adjustment were used (see Table 7).

3.4.3. *Rheological properties*

The rheological properties of the different formulations were determined to identify the influence of the yeast oil integration form on the production process and microstructure of the O/W emulsion. All VMA compositions show shear thinning flow behavior in Fig. 12, with varying degrees depending on the formulation. The direct comparison of the formulation Y0 and Y1 shows that the usage of the yeast oil in Y1 leads to

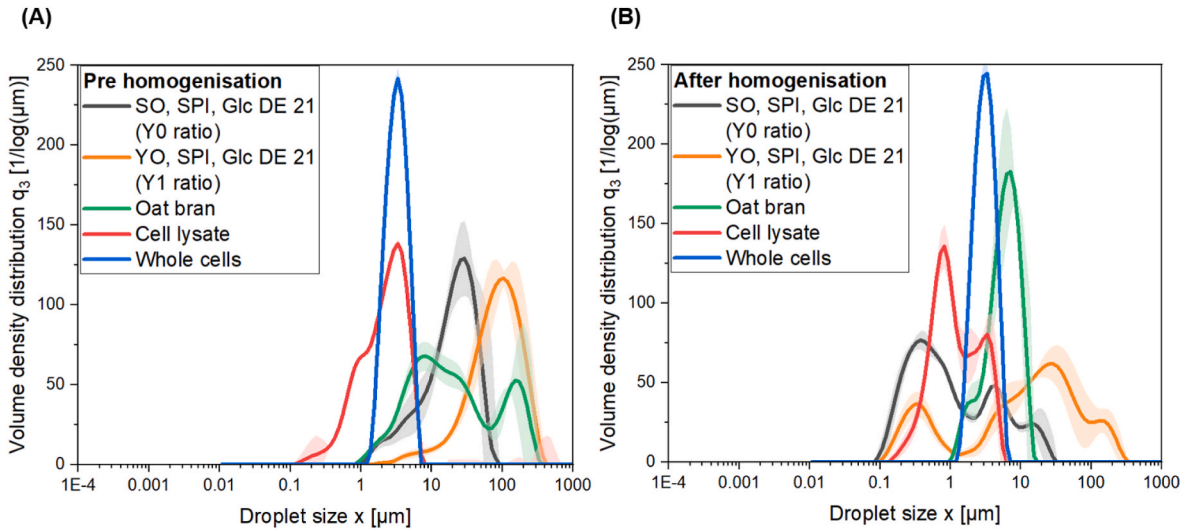

Fig. 10. Volume density distribution of the different formulation components (A) before and (B) after processing in the high-pressure homogenizer.

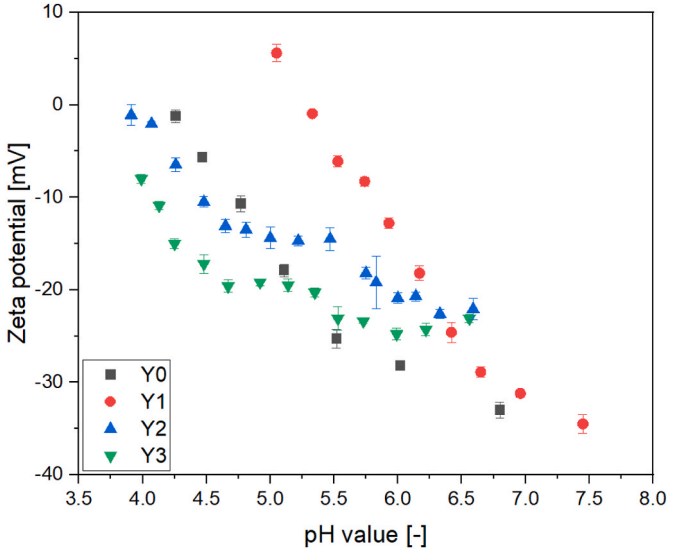

Fig. 11. Zeta potential as a function of the pH value for the formulations Y0 (reference with sunflower oil), Y1 (yeast oil), Y2 (cell lysate) and Y3 (whole cells).

Table 6
Characteristic droplet size parameters of the component analysis depending on the processing in the high-pressure homogenizer.

Components/ Pressure [bar]		$x_{10,3}$ [µm]	$x_{50,3}$ [µm]	$x_{90,3}$ [µm]	$x_{3,2}$ [µm]	$x_{4,3}$ [µm]	SPAN [−]
SO, SPI, Glc DE 21 (Y0 ratio)	Pre	4.8 ± 0.2	21.9 ± 1.0	50.0 ± 3.7	11.2 ± 2.3	25.1 ± 4.8	2.1 ± 0.2
	450/150	0.2 ± 0.0	0.8 ± 0.0	8.0 ± 0.7	0.5 ± 0.1	2.8 ± 0.2	10.4 ± 0.0
YO, SPI, Glc De 21 (Y1 ratio)	Pre	23.8 ± 8.7	84.5 ± 12.5	203.0 ±0 .31.2	42.6 ± 12.9	101.0 ± 27.3	2.1 ± 0.3
	450/150	0.3 ± 0.0	14.5 ± 1.8	95.1 ± 14.6	1.3 ± 0.2	33.0 ± 6.2	6.5 ± 3.1
Oat bran	Pre	3.5 ± 0.1	14.5 ± 1.8	119.0 ± 30.0	8.3 ± 2.1	37.0 ± 5.1	8.0 ± 2.2
	450/150	2.5 ± 0.0	5.8 ± 0.1	9.8 ± 0.4	4.6 ± 0.2	6.0 ± 1.3	1.3 ± 0.0
Cell lysate	Pre	0.7 ± 0.0	2.3 ± 0.0	4.7 ± 0.1	1.6 ± 0.1	2.5 ± 0.1	1.7 ± 0.0
	450/150	0.4 ± 0.1	1.0 ± 0.1	3.6 ± 0.3	0.9 ± 0.1	1.6 ± 0.4	3.1 ± 0.1
Whole cells	Pre	2.0 ± 0.0	3.2 ± 0.0	5.0 ± 0.0	3.0 ± 0.0	3.4 ± 0.1	0.9 ± 0.1
	450/150	1.9 ± 0.0	3.1 ± 0.0	4.7 ± 0.0	2.9 ± 0.0	3.2 ± 0.0	0.9 ± 0.0

Table 7
Overview of the pH value and the zeta potential after the homogenization process.

Formulation	pH value [−]	Zeta potential [mV]
Y0	7.19 ± 0.10	−43.76 ± 0.72
Y1	7.06 ± 0.08	−32.85 ± 0.63
Y2	6.34 ± 0.21	−22.60 ± 0.25
Y3	6.53 ± 0.15	−22.98 ± 0.19

an increase in viscosity after high-pressure homogenization compared to the reference with sunflower oil in Y0. The different fatty acid composition of the yeast oil and sunflower oil (see section 3.3) has an influence on the results of the rheological measurement. The incorporation form of the cell lysate in Y2 and the whole cells in Y3 results in a significant viscosity increase. The amount of protein and dietary fiber β-glucan is constant between formulations, but insoluble cell components such as the cell membrane as well as cell compartments can influence viscosity measurements. For whole yeast cells formulations, also the elasticity of the cells may play a role and is estimated to be around 20–30% (Mishra et al., 2022). The studies by Agbenorhevi et al. (2011) show that the oat fiber β-glucan causes the formation of highly viscous solutions, which is affected by the molecular weight, the used concentration, and the interaction with other compounds. The raw material oat bran is also characterized by a proportion of insoluble components, an effect on the measurement is to be expected. Due to the different material sources of the fiber, from oats and yeast cells, differences in the influencing parameters identified (Agbenorhevi et al., 2011) are anticipated. O'Flynn et al. (2021) were able to show in studies with soy protein isolate that protein solubility correlates with the flow behavior of the solutions. The protein solutions exhibited shear thinning flow behavior (O'Flynn et al., 2021), which was confirmed by the performed measurements. This correlation was also found in viscosity determinations of oat β-glucan (Kivelä et al., 2010). In 3.3.2, the different integration form of yeast oil affects the different pH of emulsion after homogenization and diminished the zeta potential. An influence of the different protein solubilities between the formulations is expected in the rheological study. However, since the viscosities are higher for formulations Y3 and Y4, the impact of

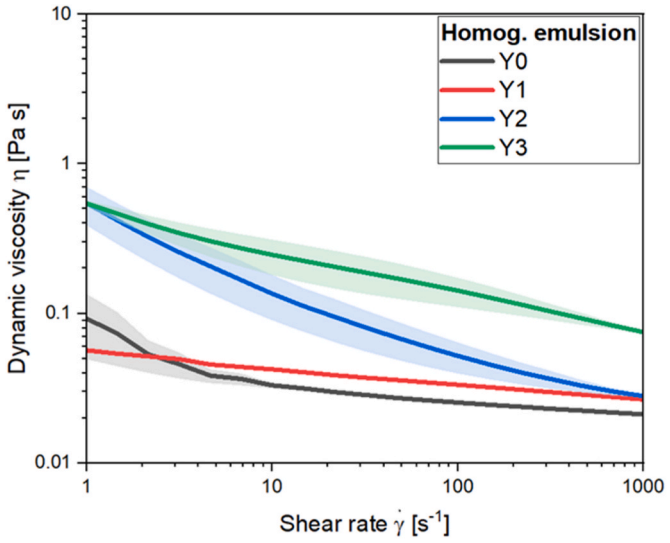

Fig. 12. Dynamic viscosity as a function of shear rate for the homogenized emulsions of formulations Y0 (reference with sunflower oil), Y1 (yeast oil), Y2 (cell lysate) and Y3 (whole cells) with a total solid content of 30%.

electrostatic repulsion of the emulsifier molecules is considered to be small. The determination of the droplet size distribution already shows that the droplet size can be reduced by introducing the oil into Y0 and Y1. Based on the single component analysis, the size reduction is due to the comminution of the oil droplets during high pressure homogenization, whereas in composition Y3 and Y4, the cell compartments, formed aggregates, oat bran and fiber are fragmented. An accumulation of the constituents at the shear plane during rheological testing can have a significant influence on the measurement results as well as on the occurring deviations. The different fatty acid profiles between sunflower oil (Y0) and yeast oil (Y1–Y3) are expected to influence the rheological behavior, as seen in 3.2.

3.4.4. Interfacial tension analysis

To understand the droplet break-up between the formulations and to identify further characteristics of the yeast oil, the interfacial tension between the oil systems and water was investigated. As the processing was conducted in the high-pressure homogenizer at a temperature of 20 °C, the temperature was kept constant during the measurement. Fig. 13 shows that the interfacial tension of sunflower oil to water is significantly lower than that of the yeast oil. Interfacial tension decreases with time, whereas the analyzed system exhibits an almost constant tension. The differences can be attributed, inter alia, to the varying fatty acid compositions and the associated disparities in lipid properties. Especially the different viscosities have a considerable influence on the measurement results, as higher viscosity values lead to stronger interactions between the molecules and reduced diffusion processes at the interface. Consequently, higher viscosities can increase interfacial tension. The decreasing tension over time using sunflower oil may be due to the presence of proteins in the raw material. Considering 3.4.1, the droplet break-up is more efficient when the sunflower oil is integrated in the formulation and results in smaller droplet diameters.

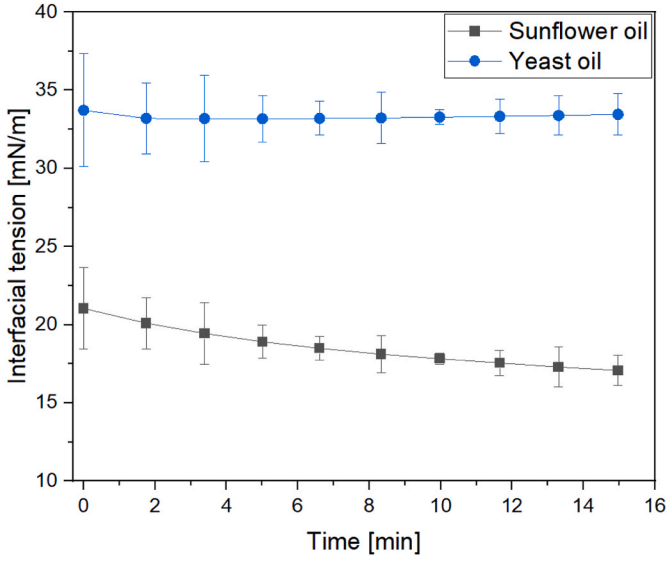

Fig. 13. Interfacial tension as a function of time for the systems sunflower oil and yeast oil to water at 20 °C.

3.5. Influence of yeast oil on the particle characteristics

In Table 8, the particle size distribution shows the smallest diameters for formulation Y0 using sunflower oil, followed by formulation Y1 with yeast oil. In consideration of 3.3.2 and 3.3.3, the lower zeta potential and higher viscosity values of the composition with yeast oil (Y1–Y3) lead to larger droplets at the nozzle tip during spray drying with constant drying parameters. Consequently, the heat and mass transfer occurring in the process depends on the composition. The integration of cell lysate and whole cells into the VMA formulations leads to larger particle diameters, which are to be expected as a result of higher viscosity values. The electron microscopic images (see Figs. 14 and 15) confirm the particle size measurements. The insertion of the whole cells in Y3 is characterized by a significantly broader particle size distribution after the spray drying process, but the Sauter mean diameter differs only slightly compared to Y2. The differences in the characteristic particle size $d_{90,3}$ between Y2 and Y3 can be attributed to the formation of agglomerates during the measurement. Formulation Y3 also exhibits morphological differences due to a plasticizing particle surface (see Fig. 15 (B)). The morphological images of Y2 in Fig. 15 (A) show that the primary particles are partially connected by sinter bridges. The formation is less pronounced compared to formulation Y3. The sintering process between primary particles is influenced by the moisture content, since the water content of Y3 is higher than Y2 sinter bridges are more pronounced. Due to the small particle sizes of the yeast cells, no complete drying of the cell interior can be assumed during the spray drying process. For VMA formulations Y0 and Y1, no significant morphological differences are recognizable in Fig. 14.

The incorporation form of the yeast oil and the whole yeast cells results in lower proportions of closed pores in the solid particle compared to the reference formulation Y0 (see Table 8). The determination of the surface lipid content indicates that formulations Y1 and Y3

Table 8
Overview of the characteristic particle properties of the spray-dried formulations Y0 (reference with sunflower oil), Y1 (yeast oil), Y2 (cell lysate) and Y3 (whole cells).

	Y0	Y1	Y2	Y3
$d_{10,3}$ [μm]	6.5 ± 0.7	6.8 ± 1.6	7.3 ± 0.3	6.8 ± 0.6
$d_{50,3}$ [μm]	24.1 ± 2.2	26.0 ± 3.9	25.3 ± 1.7	26.2 ± 3.0
$d_{90,3}$ [μm]	89.6 ± 8.1	97.0 ± 9.7	129.9 ± 12.4	219.7 ± 10.4
$d_{3,2}$ [μm]	12.9 ± 0.4	13.6 ± 2.4	13.8 ± 0.5	13.7 ± 1.2
SPAN [−]	3.5 ± 0.0	3.5 ± 0.4	4.8 ± 1.2	8.1 ± 0.4
S [−]	0.82 ± 0.0	0.81 ± 0.0	0.81 ± 0.0	0.80 ± 0 0
M_{wb} [g/100 g]	1.8 ± 0.6	2.2 ± 0.5	3.0 ± 0.4	3.2 ± 0.8
ρ_s [kg/m^3]	956.3 ± 6.4	960.0 ± 6.9	1155.3 ± 5.5	1145.7 ± 11.2
ε_{closed} [%]	11.0 ± 1.3	6.4 ± 1.1	18.1 ± 0.6	2.1 ± 0.7
Surface lipid content [%]	5.2 ± 0.1	4.7 ± 0.3	6.0 ± 0.9	2.3 ± 0.2
EE [%]	94.8 ± 0.1	95.3 ± 0.3	94.0 ± 0.9	97.7 ± 0.2

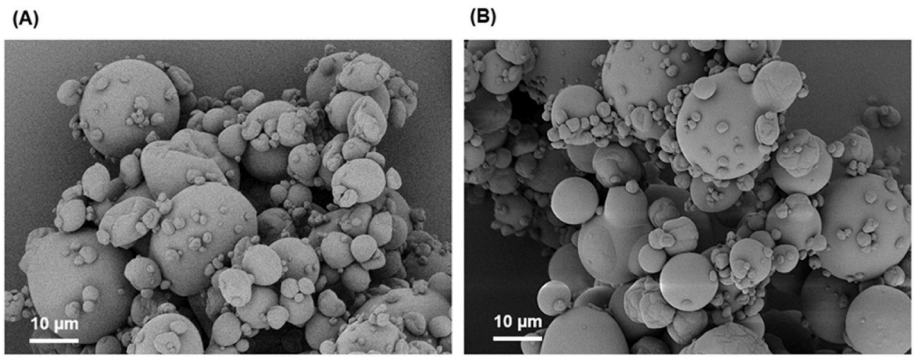

Fig. 14. Electron microscopic image of the PBMA formulations (A) Y0 and (B) Y1 at a magnification of 3kx.

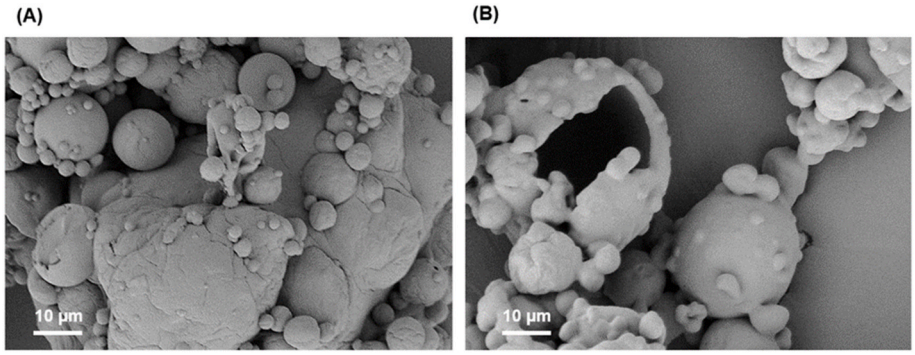

Fig. 15. Electron microscopic image of the PBMA formulations (A) Y2 and (B) Y3 at a magnification of 3kx.

have a greater amount of encapsulated oil at a constant concentration and under consideration of the moisture content after the spray drying process. Thus, the integration of sunflower oil in Y0 and the cell lysate in Y2 leads to a greater number of pores instead of lipid inclusions. The yeast compartments that are no longer present in the cell inclusion due to the digestion process can possibly have a negative influence on the encapsulation effectiveness. In OY such as *C. oleaginosus* excessive carbon is accumulated in storage molecules, mainly triglycerides, to form hydrophobic bodies. In intact cells, these bodies are stabilized by polar lipids (Zhu et al., 2015). Furthermore, an influence of the water-insoluble yeast cell wall compounds and the insoluble fiber of the oat bran on the spray-drying process and lipid encapsulation is to be expected.

Due to the low proportion of surface lipids when using the extracted yeast oil and especially the whole cells, higher oxidation stability of the powder product is to be anticipated as the microorganism also has additional antioxidants (Kim et al., 2002). In investigations by Czerniak et al. (2015), the oil encapsulated in yeast cells exhibited stability against oxidation over a period of 30 days, particularly at low relative humidities during storage.

4. Conclusion

The overall aim of the presented work, a completely novel approach, was to demonstrate the possibility of producing an oleaginous yeast-based milk powder alternative. To highlight the possible impact, the extracted yeast oil was compared to the broadly used palm oil as well as to the sunflower oil used in the reference vegan milk alternative. Starting from the fermentation, the whole process was covered, and three different formulations were tested. To conclude, an extensive analysis of the properties of the emulsions and powders derived from yeast oils, OY lysate and whole cells was performed and compared to the reference vegan milk alternative formulation.

Most remarkably, the high encapsulating efficiency and low surface lipid content of the whole cell formulation indicate a better stability compared to the reference formulation. On the other side, the droplet size of the emulsion and of the spray-dried product's particles is larger in case of the formulation with cell lysate and whole cells compared to the ones with yeast or sunflower oil. This is supported by the rheological studies, which observed a viscosity increase for formulations containing cell lysate and whole cells. For the spray-dried particles, morphological differences are observed in electron microscopic images, highlighting the impact of yeast oil integration on the spray-dried particles.

The ease of an "all-in-one" formulation using oleaginous yeast is bought with the burden of a complex system. It has to be acknowledged, that the diversity of components present in yeast cells may or may not influence all processes presented in this work in multiple ways. A detailed investigation of each phenomenon would blow up the frame of this study. Notably, this research introduces the integration of yeast oil in different forms into vegan milk alternative emulsion formulations for the first time. However, it is emphasized that further experiments are needed to fully comprehend the observed effects. Continued research and additional experiments will be crucial to unlocking the full potential and understanding the underlying mechanisms of these innovative formulations. From an economic point of view, using alternative, less refined carbon sources can reduce production costs in the future. Before commercialization, regulatory hurdles such as toxicology studies and novel food regulations must be considered.

Symbols

Latin symbols		
A	area covered by particle protection	m^2
d	particle diameter	m
d_{32}	Sauter mean diameter	m
E	Energy	J
F	Force	N
H	Enthalpy	J

(*continued on next page*)

(*continued*)

f	Heywood factor	–
L	Length	m
M	moisture content	g/g
m	Mass	g
P	circumference of the particle projection	m
p	Pressure	Pa
S	Sphericity	–
S_v	specific surface	m^{-1}
V	Volume	m^3
X	droplet diameter	m
Greek letters		
γ	interfacial tension	N m^{-1}
ε	Porosity	–
θ	phase angle	°
M	growth rate	h^{-1}
ρ	Density	kg m^{-3}

Sub- and Superscripts	
a	Ambient
c	Crushed
f	Final
i	Initial
max	Maximum
ref	Reference
s	Sample
SL	surface lipid content
TL	total lipid content
Abbreviations	
BDM	biomass dry weight
DE	dextrose equivalent
DSC	differential scanning calorimetry
EE	encapsulation effectivity
FAME	fatty acid methyl ester
FID	flame ionization detector
GC	gas chromatography
Glc	glucose syrup
HPLC	high performance liquid chromatography
LB	lysogeny broth
OB	oat bran
OD	optical density
OTR	oxygen transfer rate
O/W	oil/water
VMA	vegan milk alternative
RI	refractive index
rpm	revolutions per minute
SEM	scanning election microscope
SPI	soy protein isolate
TAG	Triacylglycerol
vvm	volume of air per volume of liquid per minute
wb	wet basis
YO	yeast oil

CRediT authorship contribution statement

K. Kramm: Writing – review & editing, Writing – original draft, Project administration, Methodology, Investigation, Funding acquisition, Conceptualization. **J. Heuer:** Writing – review & editing, Writing – original draft, Project administration, Methodology, Investigation, Funding acquisition, Conceptualization. **V. Meunier:** Writing – review & editing, Supervision, Funding acquisition. **K. Haas:** Writing – review & editing, Supervision. **P. Arbter:** Writing – review & editing, Supervision, Funding acquisition. **S. Heinrich:** Writing – review & editing, Supervision, Project administration, Funding acquisition.

Declaration of competing interest

The authors declare that they have no known competing financial interests or personal relationships that could have appeared to influence the work reported in this paper.

Data availability

Data will be made available on request.

Acknowledgment

The I^3 program of Hamburg University of Technology (TUHH) funded the project. K. Kramm is financially supported by Nestec Ltd. and would like to thank Nestlé Research and Development for the assistance. J. Heuer is financially supported by the German Federal Ministry for Economic Affairs and Climate Action (BMWK) and the European Social Fund (ESF) via the EXIST program. The authors would like to thank Maëlle Grimault, Celina Nahrgang and Simge Korkmaz for their support with the measurements.

References

Agbenorhevi, J.K., Kontogiorgos, V., Kirby, A.R., Morris, V.J., Tosh, S.M., 2011. Rheological and microstructural investigation of oat β-glucan isolates varying in molecular weight. Int. J. Biol. Macromol. 49 (3), 369–377. https://doi.org/10.1016/j.ijbiomac.2011.05.014.

Ali, A.H., Zou, X., Abed, S.M., Korma, S.A., Jin, Q., Wang, X., 2019. Natural phospholipids: occurrence, biosynthesis, separation, identification, and beneficial health aspects. Crit. Rev. Food Sci. Nutr. 59 (2), 253–275. https://doi.org/10.1080/10408398.2017.1363714.

Aliyu, H., Gorte, O., Neumann, A., Ochsenreither, K., 2021. Global transcriptome profile of the oleaginous yeast *Saitozyma podzolica* DSM 27192 cultivated in glucose and xylose. Journal of Fungi (Basel, Switzerland) 7 (9). https://doi.org/10.3390/jof7090758.

Arbter, P., Sinha, A., Troesch, J., Utesch, T., Zeng, A.-P., 2019. Redox governed electro-fermentation improves lipid production by the oleaginous yeast *Rhodosporidium toruloides*. Bioresour. Technol. 294, 122122 https://doi.org/10.1016/j.biortech.2019.122122.

Armbruster, H., Karbstein, H., Schubert, H., 1991. Herstellung von Emulsionen unter Berücksichtigung der Grenzflächenbesetzungskinetik des Emulgators. Chem. Ing. Tech. 63 (3), 266–267. https://doi.org/10.1002/cite.330630323.

Athenaki, M., Gardeli, C., Diamantopoulou, P., Tchakouteu, S.S., Sarris, D., Philippoussis, A., Papanikolaou, S.[S., 2018. Lipids from yeasts and fungi: physiology, production and analytical considerations. J. Appl. Microbiol. 124 (2), 336–367. https://doi.org/10.1111/jam.13633.

Beopoulos, A., Nicaud, J.-M., Gaillardin, C., 2011. An overview of lipid metabolism in yeasts and its impact on biotechnological processes. Appl. Microbiol. Biotechnol. 90 (4), 1193–1206. https://doi.org/10.1007/s00253-011-3212-8.

Blomqvist, J., Pickova, J., Tilami, S.K., Sampels, S., Mikkelsen, N., Brandenburg, J., Sandgren, M., Passoth, V., 2018. Oleaginous yeast as a component in fish feed. Sci. Rep. 8 (1), 15945 https://doi.org/10.1038/s41598-018-34232-x.

Cardello, A.V., Llobell, F., Giacalone, D., Roigard, C.M., Jaeger, S.R., 2022. Plant-based alternatives vs dairy milk: consumer segments and their sensory, emotional, cognitive and situational use responses to tasted products. Food Qual. Prefer. 100, 104599 https://doi.org/10.1016/j.foodqual.2022.104599.

Caruso, M.A., Piermaria, J.A., Abraham, A.G., Medrano, M., 2022. β-glucans obtained from beer spent yeasts as functional food grade additive: focus on biological activity. Food Hydrocolloids 133, 107963. https://doi.org/10.1016/j.foodhyd.2022.107963.

Colombo, A.L., Padovan, A.C.B., Chaves, G.M., 2011. Current knowledge of *Trichosporon spp.* and *Trichosporonosis*. Clin. Microbiol. Rev. 24 (4), 682–700. https://doi.org/10.1128/cmr.00003-11.

Czerniak, A., Kubiak, P., Białas, W., Jankowski, T., 2015. Improvement of oxidative stability of menhaden fish oil by microencapsulation within biocapsules formed of yeast cells. J. Food Eng. 167, 2–11. https://doi.org/10.1016/j.jfoodeng.2015.01.002.

Di Fidio, N., Minonne, F., Antonetti, C., Raspolli Galletti, A.M., 2021. *Cutaneotrichosporon oleaginosus*: a versatile whole-cell biocatalyst for the production of single-cell oil from agro-industrial wastes. Catalysts 11 (11), 1291. https://doi.org/10.3390/catal11111291.

Geburt, K., Albrecht, E.H., Pointke, M., Pawelzik, E., Gerken, M., Traulsen, I., 2022. A comparative analysis of plant-based milk alternatives Part 2: environmental impacts. Sustainability 14 (14), 8424. https://doi.org/10.3390/su14148424.

Gong, Z., Zhou, W., Shen, H., Yang, Z., Wang, G., Zuo, Z., Hou, Y., Zhao, Z.K., 2016a. Co-fermentation of acetate and sugars facilitating microbial lipid production on acetate-rich biomass hydrolysates. Bioresour. Technol. 207, 102–108. https://doi.org/10.1016/j.biortech.2016.01.122.

Gong, Z., Zhou, W., Shen, H., Zhao, Z.K., Yang, Z., Yan, J., Zhao, M., 2016b. Co-utilization of corn stover hydrolysates and biodiesel-derived glycerol by *Cryptococcus curvatus* for lipid production. Bioresour. Technol. 219, 552–558. https://doi.org/10.1016/j.biortech.2016.08.021.

Griffiths, M.J., van Hille, R.P., Harrison, S.T.L., 2010. Selection of direct transesterification as the preferred method for assay of fatty acid content of microalgae. Lipids 45 (11), 1053–1060. https://doi.org/10.1007/s11745-010-3468-2.

Gujjari, P., Suh, S.-O., Coumes, K., Zhou, J.J., 2011. Characterization of oleaginous yeasts revealed two novel species: *Trichosporon cacaoliposimilis sp.* Nov. And *Trichosporon oleaginosus sp.* Nov. Mycologia 103 (5), 1110–1118. https://doi.org/10.3852/10-403.

Haas, R., Schnepps, A., Pichler, A., Meixner, O., 2019. Cow milk versus plant-based milk substitutes: a comparison of product image and motivational structure of consumption. Sustainability 11 (18), 5046. https://doi.org/10.3390/su11185046.

Hu, M., McClements, D.J., Decker, E.A., 2003. Lipid oxidation in corn oil-in-water emulsions stabilized by casein, whey protein isolate, and soy protein isolate. J. Agric. Food Chem. 51 (6), 1696–1700. https://doi.org/10.1021/jf020952j.

Kim, E.H.-J., Chen, X., Pearce, D., 2002. Surface characterization of four industrial spray-dried dairy powders in relation to chemical composition, structure and wetting property. Colloids Surf. B Biointerfaces 26 (3), 197–212. https://doi.org/10.1016/S0927-7765(01)00334-4.

Kivelä, R., Pitkänen, L., Laine, P., Aseyev, V., Sontag-Strohm, T., 2010. Influence of homogenisation on the solution properties of oat β-glucan. Food Hydrocolloids 24 (6–7), 611–618. https://doi.org/10.1016/j.foodhyd.2010.02.008.

Koivuranta, K., Castillo, S., Jouhten, P., Ruohonen, L., Penttilä, M., Wiebe, M.G., 2018. Enhanced triacylglycerol production with genetically modified *Trichosporon oleaginosus*. Front. Microbiol. 9, 1337. https://doi.org/10.3389/fmicb.2018.01337.

Kourist, R., Bracharz, F., Lorenzen, J., Kracht, O.N., Chovatia, M., Daum, C., Deshpande, S., Lipzen, A., Nolan, M., Ohm, R.A., Grigoriev, I.V., Sun, S., Heitman, J., Brück, T., Nowrousian, M., 2015. Genomics and transcriptomics analyses of the oil-accumulating basidiomycete yeast *Trichosporon oleaginosus*: insights into substrate utilization and alternative evolutionary trajectories of fungal mating systems. mBio 6 (4), e00918. https://doi.org/10.1128/mbio.00918-15.

Kramm, K., Roucher, A., Busom Descarrega, J., Ambühl, M., Kammerhofer, J., Meunier, V., Heinrich, S., 2024. Influence of material characteristics on plant-based milk alternative properties. J. Food Eng. 373, 112019. https://doi.org/10.1016/j.jfoodeng.2024.112019. ISSN 0260-8774.

Kregiel, D., Berlowska, J., Szubzda, B., 2012. Novel permittivity test for determination of yeast surface charge and flocculation abilities. J. Ind. Microbiol. Biotechnol. 1881–1886.

Leal-Calderon, F., Schmitt, V., Bibette, J., 2007. Emulsion Science: Basic Principles, vol. 2. Springer Science+Business Media. https://doi.org/10.1007/978-0-387-39683-5.

Li, Q., Du, W., Liu, D., 2008. Perspectives of microbial oils for biodiesel production. Appl. Microbiol. Biotechnol. 80 (5), 749–756. https://doi.org/10.1007/s00253-008-1625-9.

Lourenço, S.C., Moldão-Martins, M., Alves, V.D., 2019. Antioxidants of natural plant origins: from sources to food industry applications. Molecules 24 (22). https://doi.org/10.3390/molecules24224132.

Márquez, A.L., Pérez, M.P., Wagner, J.R., 2013. Solid fat content estimation by differential scanning calorimetry: prior treatment and proposed correction. J. Am. Oil Chem. Soc. 90 (4), 467–473. https://doi.org/10.1007/s11746-012-2190-z.

Meng, X., Yang, J., Xu, X., Zhang, L., Nie, Q., Xian, M., 2009. Biodiesel production from oleaginous microorganisms. Renew. Energy 34 (1), 1–5. https://doi.org/10.1016/j.renene.2008.04.014.

Mie, G., 1908. Beiträge zur Optik trüber Medien, speziell kolloidaler Metallösungen. Ann. Phys. 330 (3), 377–445. https://doi.org/10.1002/andp.19083300302.

Mishra, R., Minc, N., Peter, M., 2022. Cells under pressure: how yeast cells respond to mechanical forces. Trends Microbiol. 30 (5), 495–510. https://doi.org/10.1016/j.tim.2021.11.006.

Moon, N.J., Hammond, E.G., Glatz, B.A., 1978. Conversion of cheese whey and whey permeate to oil and single-cell protein. J. Dairy Sci. 61 (11), 1537–1547. https://doi.org/10.3168/jds.S0022-0302(78)83762-X.

Ochsenreither, K., Glück, C., Stressler, T., Fischer, L., Syldatk, C., 2016. Production strategies and applications of microbial single cell oils. Front. Microbiol. 7, 1539. https://doi.org/10.3389/fmicb.2016.01539.

O'Flynn, T.D., Hogan, S.A., Daly, D.F.M., O Mahony, J.A., McCarthy, N.A., 2021. Rheological and solubility properties of soy protein isolate. Molecules 26 (10). https://doi.org/10.3390/molecules26103015.

Papanikolaou, S., Seraphim, Aggelis, G., 2011. Lipids of oleaginous yeasts. Part I: biochemistry of single cell oil production. Eur. J. Lipid Sci. Technol. 113 (8), 1031–1051. https://doi.org/10.1002/ejlt.201100014.

Reyes-Jurado, F., Soto-Reyes, N., Dávila-Rodríguez, M., Lorenzo-Leal, A.C., Jiménez-Munguía, M.T., Mani-López, E., López-Malo, A., 2023. Plant-based milk alternatives: types, processes, benefits, and characteristics. Food Rev. Int. 39 (4), 2320–2351. https://doi.org/10.1080/87559129.2021.1952421.

Romulo, Andreas, 2022. IOP Conf. Ser.: Earth Environ. Sci. 998, 012054 https://doi.org/10.1088/1755-1315/998/1/012054.

Sitepu, I.R., Sestric, R., Ignatia, L., Levin, D., German, J.B., Gillies, L.A., Almada, L.A.G., Boundy-Mills, K.L., 2013. Manipulation of culture conditions alters lipid content and fatty acid profiles of a wide variety of known and new oleaginous yeast species. Bioresour. Technol. 144, 360–369. https://doi.org/10.1016/j.biortech.2013.06.047.

Stirke, A., Celiesiute-Germaniene, R., Zimkus, A., Zurauskiene, N., Simonis, P., Dervinis, A., Ramanavicius, A., Balevicius, S., 2019. The link between yeast cell wall porosity and plasma membrane permeability after PEF treatment. Sci. Rep. 9 (1) https://doi.org/10.1038/s41598-019-51184-y.

Subramaniam, R., Dufreche, S., Zappi, M., Bajpai, R., 2010. Microbial lipids from renewable resources: production and characterization. J. Ind. Microbiol. Biotechnol. 37 (12), 1271–1287. https://doi.org/10.1007/s10295-010-0884-5.

Tomczynska-Mleko, M., Kamysz, E., Sikorska, E., Puchalski, C., Mleko, S., Ozimek, L., Kowaluk, G., Gustaw, W., Wesolowska-Trojanowska, M., 2014. Changes of secondary structure and surface tension of whey protein isolate dispersions upon pH and temperature. Czech J. Food Sci. 32 (1), 82–89. https://doi.org/10.17221/326/2012-CJFS.

Wei, Y., Siewers, V., Nielsen, J., 2017. Cocoa butter-like lipid production ability of non-oleaginous and oleaginous yeasts under nitrogen-limited culture conditions. Appl. Microbiol. Biotechnol. 101 (9), 3577–3585. https://doi.org/10.1007/s00253-017-8126-7.

Wolf, W.J., 1970. Soybean proteins. Their functional, chemical, and physical properties. J. Agric. Food Chem. 18 (6), 969–976. https://doi.org/10.1021/jf60172a025.

Yu, X., Zeng, J., Zheng, Y., Chen, S., 2014a. Effect of lignocellulose degradation products on microbial biomass and lipid production by the oleaginous yeast *Cryptococcus curvatus*. Process Biochem. 49 (3), 457–465. https://doi.org/10.1016/j.procbio.2013.10.016.

Yu, X., Zheng, Y., Xiong, X., Chen, S., 2014b. Co-utilization of glucose, xylose and cellobiose by the oleaginous yeast *Cryptococcus curvatus*. Biomass Bioenergy 71, 340–349. https://doi.org/10.1016/j.biombioe.2014.09.023.

Zhang, X., Zhang S, Shuang, Xie, F., Han, L., Li, L., Jiang, L., Qi, B., Li, Y., 2021. Soy/whey protein isolates: interfacial properties and effects on the stability of oil-in-water emulsions. J. Sci. Food Agric. 101 (1), 262–271. https://doi.org/10.1002/jsfa.10638.

Zhu, Z., Ding, Y., Gong, Z., Yang, L., Zhang S, Sufang, Zhang, C., Lin, X., Shen, H., Zou, H., Xie, Z., Yang, F., Zhao, X., Liu, P., Zhao, Z.K., 2015. Dynamics of the lipid droplet proteome of the Oleaginous yeast *rhodosporidium toruloides*. Eukaryot. Cell 14 (3), 252–264. https://doi.org/10.1128/ec.00141-14.

Zweytick, D., Athenstaedt, K., Daum, G., 2000. Intracellular lipid particles of eukaryotic cells. Biochim. Biophys. Acta 1469 (2), 101–120. https://doi.org/10.1016/s0005-2736(00)00294-7.